DALTON

The preparation and crystal and molecular structures of new luminescent Schiff-base complexes featuring coupled lanthanide(III) cations

Robertha C. Howell,[a] Kirk V. N. Spence,[a] Ishenkumba A. Kahwa,*[a] Andrew J. P. White[b] and David J. Williams[b]

[a] *Chemistry Department, University of the West Indies, Mona, Kingston 7, Jamaica*
[b] *Chemistry Department, Chemical Crystallography Laboratory, Imperial College of Science, Technology and Medicine, South Kensington, London SW7 2AY, UK*

The reaction between salicylaldehyde, diethylenetriamine and lanthanide(III) (Ln^{3+}) nitrates in refluxing methanol produced new acyclic dimeric Schiff-base compounds $[\{LnL^7(NO_3)\}_2]$ (H_2L^7 is the 2:1 Schiff-base condensation product of salicylaldehyde and diethylenetriamine) in which the coupled Ln^{3+} ions are bridged by phenolate groups and separated by a short Ln ··· Ln distance of *ca.* 3.81 Å. In contrast with lanthanide(III) dinuclear macrocyclic compounds of Schiff bases studied previously where the ligand negative charge to Ln^{3+} cation ratio is 1:1, chelate L^7 possess a higher ratio of 2:1. The dimeric compounds of L^7 feature a shorter Ln^{3+} ··· Ln^{3+} separation, greater stability and enhanced electronic coupling among Ln^{3+}–Ln^{3+} ion pairs. For example, $[\{LnL^7(NO_3)\}_2]$ complexes readily yielded intact dimeric species such as $[\{EuL^7\}_2]^+$ and $[Eu_2L^7{}_2(NO_3)]^+$ during fast atom bombardment mass spectrometric analyses and exhibit Eu^{3+}–Eu^{3+} and Tb^{3+}–Tb^{3+} energy migration while macrocyclic analogues do not. However, like other phenolate Schiff-base chelates, L^7 is a good sensitizer for Tb^{3+} and Eu^{3+} emission. Metal-to-ligand back-energy transfer is consistent with the temperature evolution of the Eu^{3+} ($^5D_0$) and Tb^{3+} ($^5D_4$) luminescence decay rates. Heteropair Eu^{3+}–Dy^{3+} interactions are observed; assuming a dominant dipole–dipole $Eu^{3+} \longrightarrow Dy^{3+}$ energy transfer mechanism the coupling constant is *ca.* 7×10^{-52} m^6 s^{-1}.

Crystallographic,[1-3] extensive spectroscopic[4] and luminescence decay dynamic studies[1,2,5-7] have shown that macrocyclic chelates having a pair of identical juxtaposed 18-membered co-ordination cavities (*e.g.* L^1–L^3, L^5 and L^6) are versatile dinucleating agents for lanthanide(III) cations (Ln^{3+}). What is not clear is why the macrocyclic chelate L^4 which has a pair of identical 15-membered cavities each with the potential to accommodate one Ln^{3+} cation, without apparent steric strains,[8-10] is unable to utilize both of these cavities simultaneously to produce dinuclear Ln^{3+} compounds.

One possible explanation is that dinucleation of Ln^{3+} cations by compartmental chelates (L^{2-}) such as L^1–L^6 is a two-step process [equation (1), solvent molecules omitted for clarity]

$$Ln^{3+} + L^{2-} \rightleftharpoons LnL^+ \quad (1a)$$

$$LnL^+ + Ln^{3+} \rightleftharpoons Ln_2L^{4+} \quad (1b)$$

rather than a concerted single step requiring cooperative action by a pair of Ln^{3+} cations [equation (2)].

$$2Ln^{3+} + L^{2-} \rightleftharpoons Ln_2L^{4+} \quad (2)$$

Under the regime described by equations (1a) and (1b) the second Ln^{3+} cation may be admitted into the non-metallated cavity of the LnL^+ species [equation (1a)] depending on the contribution of process (1b) to the free energy of the dinucleation process.[11] Thus, the mononucleating behaviour of potentially dinucleating chelates such as L^4, may be rationalized in terms of the stepwise complexation mechanism described by equations (1a) and (1b). Under some conditions this mechanism may not hold; results of steady-state competitive heterolanthanide cation pair complexation studies with chelate L^1 are symptomatic of a concerted Ln^{3+} dinucleation mechanism in which the co-operative behaviour of a pair of Ln^{3+} cations is important.[7] The mechanism for the dinucleation process is thus poorly understood. Factors, such as repulsive Ln^{3+} ··· Ln^{3+} and attractive ligand–Ln^{3+}

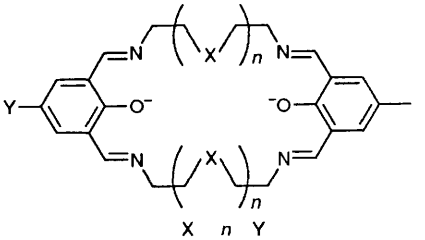

	X	*n*	Y
L^1	O	2	Me
L^2	NH	2	Me
L^3	NH	2	Cl
L^4	NH	1	Cl

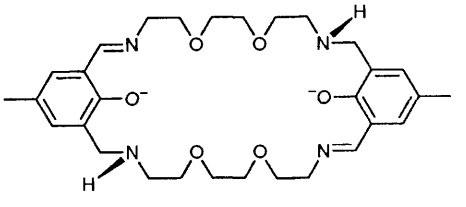

L^5

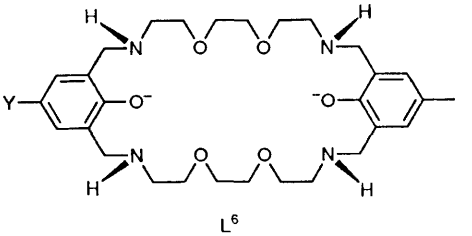

L^6

interactions as well as ligand flexibility, which depend significantly on the nature of the co-ordination cavities, are expected to feature prominently in the molecular recognition processes governing Ln^{3+} dinucleation.[11] Because of our interest in these fundamental phenomena and the potential benefits of tunable, electronically coupled homodinuclear $Ln^{3+} \cdots Ln^{3+}$ or heterodinuclear $Ln^{3+} \cdots Ln'^{3+}$ pairs[1,2,7] to magnetic resonance imaging[12] and luminescent biomedical diagnostics[13] applications, we have initiated a systematic study of the synthesis, structure and spectroscopic properties of Ln^{3+} complexes of flexible chelates[14] such as L^7–L^{12} and their cyclic analogues L^{13}–L^{18}.

It is hoped that these studies will provide valuable information on factors governing the Ln^{3+} dinucleation process, and insight into how systems featuring strongly electronically coupled $Ln^{3+} \cdots Ln^{3+}$ and $Ln^{3+} \cdots Ln'^{3+}$ species may be designed and prepared.[1]

Herein we report the syntheses, structure and luminescence characteristics of dimeric Ln^{3+} complexes of L^7. Remarkably, the dimerization of $LnL^7(NO_3)$ produces $[\{LnL^7(NO_3)\}_2]$ complexes featuring shorter intramolecular $Ln^{3+} \cdots Ln^{3+}$ separation, greater stability and stronger electronic interactions than found in dinuclear complexes of chelates L^1–L^3.

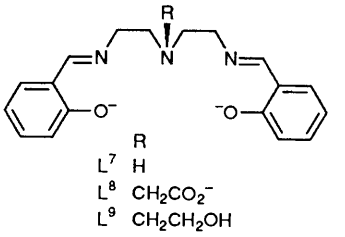

R
L^7 H
L^8 $CH_2CO_2^-$
L^9 CH_2CH_2OH

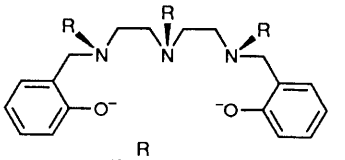

R
L^{10} H
L^{11} $CH_2CO_2^-$
L^{12} CH_2CH_2OH

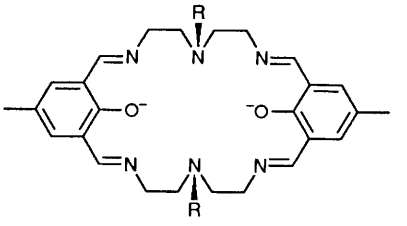

R
L^{13} H
L^{14} $CH_2CO_2^-$
L^{15} CH_2CH_2OH

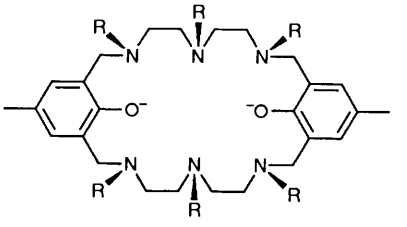

R
L^{16} H
L^{17} $CH_2CO_2^-$
L^{18} CH_2CH_2OH

Experimental

Materials

The reagents, purity and source are: salicylaldehyde 99%, BDH; diethylenetriamine 97%, BDH; gadolinium nitrate pentahydrate 99.5%, and lanthanide(III) oxides (Sm_2O_3, Eu_2O_3, Gd_2O_3, Tb_4O_7, Dy_2O_3, Ho_2O_3, Er_2O_3, Yb_2O_3, Lu_2O_3, Y_2O_3; 99.9, 99.95, 99.9, 99.999, 99.99, 99.9, 99.99, 99.99, 99.99 and 99.999% respectively), which were treated with HNO_3 to obtain the lanthanide(III) nitrates, were obtained from Aldrich. For the luminescence experiments the 99.99% (or higher) pure lanthanide oxides were used.

Elemental analysis

Nuclear activation analyses (NAA) were obtained using facilities at the UWI centre for Nuclear Sciences.[7] Carbon, hydrogen and nitrogen analyses were performed by Medac Ltd., Brunel University, Uxbridge, UK. Inductively coupled plasma (ICP) analyses were performed at the Consolidated Instruments Facility, Tulane University (samarium–europium sample) and MEDAC (lutetium sample).

Luminescence spectral and decay rate measurements

The Perkin-Elmer LS-5 luminescence spectrometer, the Photon Technology PL2300 nitrogen and PL201 dye lasers, the liquid-nitrogen cryostat, the electronic support and the inhouse computational programs were described previously.[1,7]

Spectroscopic analysis

The fast atom bombardment (glycerol matrix) mass spectral data were recorded on a Kratos Concept 1H spectrometer (Tulane University) operating in the positive-ion mode. The Perkin-Elmer 1600 series FT-IR spectrometer was described previously.[7] The HP8451A diode array spectrophotometer was used to obtain electronic absorption spectra of samples thoroughly mulled in Nujol.[6]

Preparations

The compounds are best prepared as follows: salicylaldehyde (2 mmol) was added to methanol (200 cm^3) followed by lanthanide nitrate (1 mmol) and the resulting mixture was heated for 1 h at *ca.* 60 °C. An excess of diethylenetriamine (4 mmol) was then introduced and the solution was refluxed for approximately four days to complete the precipitation process the onset of which was visible within three days. The crystalline products were harvested and dried on filter paper (Yield = 32, 22, 24, 32, 27, 23, 17, 27 and 34% for Ln = Sm, Eu, Gd, Tb, Dy, Ho, Er, Yb and Lu respectively; densities ($g\ cm^{-3}$) = 1.77, 1.77, 1.79, 1.88 for Ln = Sm, Tb, Gd and Yb respectively). The crystals appeared to crack on prolonged exposure to the atmosphere, while samples kept in the mother-liquor did not show visible signs of deterioration. In an attempt to improve crystal quality, preparation of one sample of the gadolinium compound employed salicylaldehyde, available as a tin complex, which was formed by slowly adding salicylaldehyde (4 mmol)to $SnCl_4$ (1 mmol) in benzene (150 cm^3) and stirring until evolution of HCl stopped ($\approx$4 h). The resulting compound is very air sensitive and was thus used *in situ* in the above preparation. Samples obtained from the two methods are similar. Elemental analyses are consistent with the formulations $[\{LnL^7(NO_3)\}_2]$ (Ln = Sm–Tb) and $[LnL^7(NO_3)]_2 \cdot MeOH$ (Ln = Dy–Lu) [Found (Ln = Eu): C, 41.25; H, 3.70; N, 10.50. $C_{36}H_{38}Eu_2N_8O_{10}$ requires C, 41.3; H, 3.8; N, 10.7%. Found (Ln = Tb): C, 40.80; H, 3.60; N, 10.55. $C_{36}H_{38}N_8O_{10}Tb_2$ requires C, 40.8; H, 3.6; N, 10.6%. Found (Ln = Er): C, 39.95; H, 3.55; N, 10.35. $C_{36}H_{38}Er_2N_8O_{10}$ requires C, 40.10; H, 3.8; N, 10.1%].

Table 1 Crystallographic data for $[\{LnL^7(NO_3)\}_2]$*

	Ln = Gd	Tb
Empirical formula	$C_{36}H_{38}Gd_2N_8O_{10}$	$C_{36}H_{38}N_8O_{10}Tb_2$
M	1057.2	1060.6
Colour, habit	Yellow, orange prisms	Yellow, rhombs
Radiation (λ/Å)	Mo-Kα (0.710 73)	Cu-Kα (1.541 78)
Crystal size/mm	0.20 × 0.33 × 0.50	0.04 × 0.14 × 0.21
a/Å	12.886(4)	12.908(7)
b/Å	11.894(3)	11.912(3)
c/Å	13.738(4)	13.713(8)
β/°	110.19(2)	109.86(2)
U/Å^3	1976(1)	1983(2)
μ/mm^{-1}	3.39	17.86
F(000)	1036	1040
2θ range/°	0–53	3–120
Independent reflections (R_{int})	4092	2954
Obs. reflections [$F_o > 4\sigma(F_o)$]	3546	2305
No. of parameters refined	253	254
R	0.022	0.0491
R'	0.024	0.050
Max., min. transmission	0.645, 0.479	0.3419, 0.0758
Largest difference peak, hole/e Å^{-3}	0.69, −0.41	1.04, −0.81
Largest and mean Δ/σ	0.002, 0.001	0.022, 0.003

* Details in common: monoclinic, space group $P2_1/n$; $Z = 2$; $D_c = 1.78$ g cm^{-3}; $w^{-1} = \sigma^2(F) + 0.0005F^2$.

Crystallography

Data for the gadolinium complex $[\{GdL^7(NO_3)\}_2]$ and for the isomorphous terbium compound were measured on a Siemens P4 diffractometer using ω scans. The data for both were corrected for Lorentz and polarization factors, and empirically for absorption.

The structure of the gadolinium complex $[\{GdL^7(NO_3)\}_2]$ was solved by direct methods and the non-hydrogen atoms refined anisotropically. A ΔF map revealed the positions of all the non-hydrogen atoms. The positions of all the hydrogen atoms were idealized (C,N–H = 0.96 Å), assigned isotropic thermal parameters, $U(H) = 1.2U_{eq}(C,N)$, and allowed to ride on their parent C,N atoms. The structure of the terbium complex $[\{TbL^7(NO_3)\}_2]$ was solved by replacing the Gd with Tb and refining using the atomic positions derived from the Gd complex. Refinement was by full-matrix least squares. A summary of the crystal data, data collection and refinement parameters is given in Table 1. Computations for both complexes were carried out on a 486 PC using the SHELXTL PC program system.[15]

Complete atomic coordinates, thermal parameters and bond lengths and angles have been deposited at the Cambridge Crystallographic Data Centre. See Instructions for Authors, *J. Chem. Soc., Dalton Trans.*, 1996, Issue 1.

Results and Discussion

Synthesis

The reaction between methanolic salicylaldehyde (or a tin–salicylaldehyde complex precursor) and diethylenetriamine in the presence of lanthanide(III) nitrates yields compounds with the general stoichiometry $[\{LnL^7(NO_3)\}_2]\cdot n$MeOH ($n = 0$, Ln = Sm–Tb; $n = 1$, Ln = Dy–Lu). The formation of $[\{LnL^7(NO_3)\}_2]\cdot n$MeOH is inferable from elemental, FT-IR and mass spectral analyses. No IR absorption bands due to unreacted material (NH_2 or C=O) are observed whereas HNR_2 (sharp singlet, 3300 cm^{-1}) and C=N (1642 cm^{-1}) absorptions are prominent. Remarkably, the FAB-MS spectrum of the mixed complex $[\{Sm_{0.69}Eu_{0.31}L^7(NO_3)\}_2]$ shows clustered peaks due to the intact dimers $\{(LnL^7)_2(NO_3)\}^+$, (m/z 980); $\{(Ln_2L^7_2)\cdot H_2O\}^+$, ($m/z$ 940); $\{Ln_2L^7_2\}^+$, (m/z 922) and $\{Ln_2L^7_2 - O\}^+$, (m/z 906). The parent peak at m/z 461 is due to $\{LnL^7\}^+$ and/or $\{Ln_2L^7_2\}^{2+}$. This is in sharp contrast to the behaviour of the dinuclear $[Ln_2L^2(NO_3)_4]\cdot xH_2O$ ($x = 0$, 1) complexes in which macrocycle L^2 readily lost one of the Ln^{3+} cations under FAB-MS conditions.[4] Unlike L^2, L^7 is not a dinucleating macrocycle, but it bears a chelate negative charge to Ln^{3+} cation ratio (ρ) of 2:1 compared to ρ = 1:1 for L^1. In a previous study[4] ligands without negative charges were found to be ineffective as Ln^{3+} dinucleating chelates. It is thus reasonable to expect that successful preparation of soluble and stable di- and tri-nuclear[16] Ln^{3+} complexes suitable for biomedical applications will require chelates with high ρ.

The ultimate evidence for the formation of $[\{LnL^7(NO_3)\}_2]$ was provided by a single-crystal X-ray diffraction analysis of the gadolinium(III) and terbium(III) compounds, obtained from the tin–salicylaldehyde precursor and the direct synthesis methods, respectively.

Structure of $[\{LnL^7(NO_3)\}_2]$ (Ln = Gd or Tb)

The X-ray analyses show the two structures to be isomorphous. Therefore the two different synthetic routes yield the same resultant complexes. As the geometric parameters of the two complexes do not differ significantly (Tables 2 and 3) and as the data for the gadolinium complex $[\{GdL^7(NO_3)\}_2]$ is of greater accuracy the discussion will be centred on the gadolinium complex. The gadolinium complex is dimeric with each cationic centre co-ordinated to all five ligand heteroatoms of L^7 and to two oxygen atoms of a bidentate nitrate anion (Fig. 1). One of the phenolate oxygen atoms of each ligand is binucleating and serves to bridge adjacent centres. Each Gd^{3+} cation is eight-co-ordinate with the ligating atoms forming a distorted bicapped trigonal prism, with O(1) and N(11) as the capping atoms (Fig. 2). The Gd–O,N distances (Table 4) are in the range 2.207(3) [O(21)] to 2.578(3) Å [N(8)]. The distance from the Gd^{3+} to the mononucleating phenolate oxygen atom, O(21) [2.207(3) Å] is, as expected, significantly shorter than that to the binucleating oxygen atom O(1) [2.349(2) Å] and O(1a) [2.335(2) Å]. The crystallographic centre of symmetry lies at the centre of the four membered Gd_2O_2 ring. Within this ring the non-bonded transannular Gd···Gd and O···O distances are 3.81 and 2.73 Å respectively. Comparison of this Gd_2O_2 geometry with that in the related macrocyclic dinuclear complex, $[Gd_2L^1(NO_3)_2]\cdot H_2O$ shows the Gd···Gd distance here to be significantly contracted (from 3.97 Å in the complex of L^1) while there is a commensurate increase in the O···O distance from 2.55 to 2.73 Å. The shorter Gd···Gd separation in the dinuclear complex of L^7, compared to that of L^1, is probably largely due

Table 2 Atomic coordinates (× 10^4) for $[\{GdL^7(NO_3)\}_2]$

Atom	*x*	*y*	*z*
Gd	159(1)	1575(1)	250(1)
O(1)	447(2)	−205(2)	1040(1)
C(1)	493(3)	−349(2)	2028(2)
C(2)	1440(3)	−784(3)	2758(2)
C(3)	1482(4)	−1015(3)	3755(3)
C(4)	571(4)	−831(4)	4046(3)
C(5)	−350(4)	−358(3)	3351(3)
C(6)	−407(3)	−80(3)	2339(2)
C(7)	−1396(3)	484(3)	1668(3)
N(8)	−1440(2)	1121(3)	909(2)
C(9)	−2512(3)	1628(3)	303(3)
C(10)	−2338(3)	2760(3)	−83(3)
N(11)	−1637(2)	2630(2)	−720(2)
C(12)	−1372(3)	3715(3)	−1115(3)
C(13)	−689(4)	3501(3)	−1768(4)
N(14)	307(3)	2824(2)	−1200(2)
C(15)	1102(4)	2871(3)	−1543(3)
C(16)	2145(4)	2303(3)	−1169(3)
C(17)	2859(5)	2425(5)	−1736(5)
C(18)	3866(6)	1954(6)	−1447(6)
C(19)	4228(5)	1352(5)	−555(5)
C(20)	3574(3)	1203(4)	56(4)
C(21)	2511(3)	1666(3)	−250(3)
O(21)	1896(2)	1510(2)	325(2)
N(3)	837(2)	3103(2)	2031(2)
O(31)	1085(2)	2083(2)	2131(2)
O(32)	267(3)	3427(2)	1129(2)
O(33)	1120(3)	3751(2)	2759(2)

Table 3 Atomic coordinates (× 10^4) for $[\{TbL^7(NO_3)\}_2]$

Atom	*x*	*y*	*z*
Tb	151(1)	1568(1)	250(1)
O(1)	442(5)	−203(4)	1042(4)
C(1)	497(8)	−358(7)	2033(6)
C(2)	1451(8)	−790(8)	2757(6)
C(3)	1494(10)	−1023(9)	3756(7)
C(4)	600(11)	−830(9)	4049(7)
C(5)	−352(10)	−363(9)	3350(7)
C(6)	−393(8)	−90(7)	2340(6)
C(7)	−1384(8)	477(8)	1672(7)
N(8)	−1430(5)	1085(6)	907(6)
C(9)	−2507(7)	1613(9)	300(8)
C(10)	−2330(8)	2752(8)	−65(8)
N(11)	−1628(6)	2617(6)	−705(6)
C(12)	−1369(9)	3704(7)	−1092(8)
C(13)	−679(9)	3510(8)	−1752(8)
N(14)	303(6)	2818(6)	−1194(6)
C(15)	1099(11)	2856(9)	−1536(8)
C(16)	2145(10)	2304(8)	−1159(8)
C(17)	2874(12)	2424(11)	−1715(10)
C(18)	3899(13)	1963(14)	−1417(14)
C(19)	4234(11)	1343(10)	−518(12)
C(20)	3563(8)	1201(9)	83(9)
C(21)	2512(7)	1662(8)	−238(8)
O(21)	1862(5)	1501(5)	341(4)
N(3)	816(6)	3096(6)	2019(6)
O(31)	1070(6)	2064(5)	2129(4)
O(32)	264(6)	3407(5)	1119(5)
O(33)	1114(6)	3748(5)	2762(5)

to the reduction in Gd^{3+} co-ordination from ten in L^1 to eight in L^7 with a consequent 'opening up' of the bond angles at each Gd^{3+} cation (Table 5). Each acyclic Schiff-base ligand has an essentially flat conformation with the Gd^{3+} cation and the co-ordinating atoms N(8), N(11), N(14) and O(21) are coplanar to within 0.05 Å; O(1) lies 1.03 Å from this plane. This latter deviation is due to the rotation of the phenolate ring out of the plane of the rest of the ligand by approximately 25° about the C(6)–C(7) bond to facilitate the bridging of the phenolate oxygen to the adjacent Gd^{3+} centre. In contrast, there is only a very small out of plane rotation of the other phenolate ring, *ca.*

Table 4 Selected bond lengths (Å) for $[\{LnL^7(NO_3)\}_2]$ (Ln = Gd or Tb)

	Ln = Gd	Tb
Ln–O(1)	2.349(2)	2.342(5)
Ln–N(11)	2.565(3)	2.548(7)
Ln–O(21)	2.207(3)	2.170(7)
Ln–O(32)	2.494(3)	2.475(6)
Ln–O(1a)	2.335(2)	2.338(5)
C(6)–C(7)	1.454(4)	1.461(12)
N(14)–C(15)	1.269(7)	1.267(17)
C(21)–O(21)	1.311(6)	1.350(14)
Ln–N(8)	2.578(3)	2.561(8)
Ln–N(14)	2.544(3)	2.537(8)
Ln–O(31)	2.519(2)	2.514(6)
Ln · · · Ln(a)	3.805(1)	3.797(2)
O(1)–C(1)	1.348(4)	1.349(10)
C(7)–N(8)	1.273(5)	1.259(12)
C(15)–C(16)	1.431(6)	1.430(17)

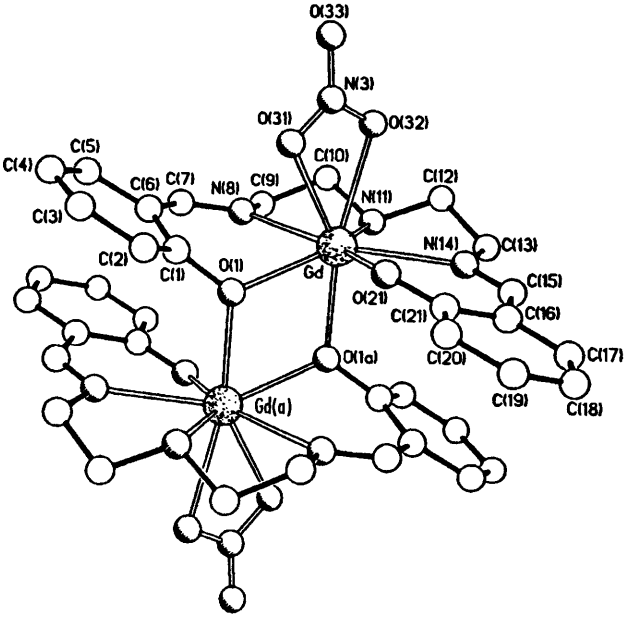

Fig. 1 The molecular structure of $[\{GdL^7(NO_3)\}_2]$

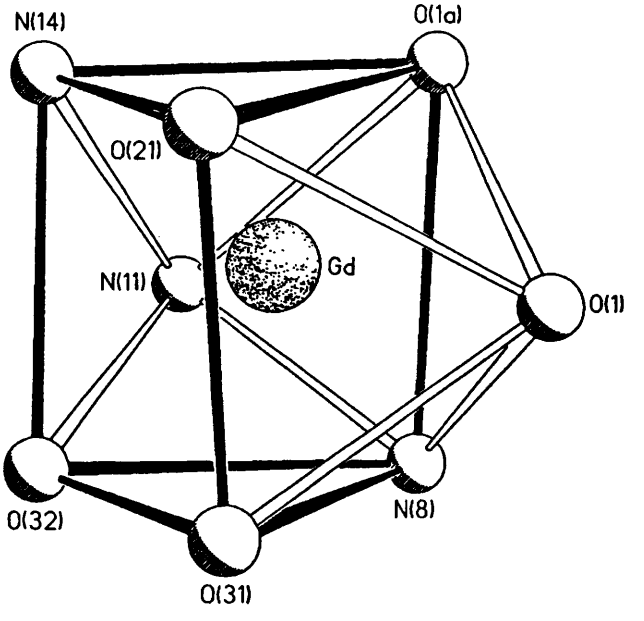

Fig. 2 The eight-fold bicapped trigonal-prismatic geometry of the co-ordination polyhedron around Gd^{3+} in $[\{GdL^7(NO_3)\}_2]$

Table 5 Selected bond angles (°) for $[\{LnL^7(NO_3)\}_2]$ (Ln = Gd or Tb)

	Ln = Gd	Tb		Ln = Gd	Tb
O(1)–Ln–N(8)	70.5(1)	69.8(2)	O(1)–Ln–N(11)	130.6(1)	130.7(2)
N(8)–Ln–N(11)	66.3(1)	66.7(3)	O(1)–Ln–N(14)	147.7(1)	147.8(2)
N(8)–Ln–N(14)	133.0(1)	133.5(2)	N(11)–Ln–N(14)	66.8(1)	66.9(3)
O(1)–Ln–O(21)	87.2(1)	86.7(2)	N(8)–Ln–O(21)	153.8(1)	152.7(2)
N(11)–Ln–O(21)	139.5(1)	140.2(3)	N(14)–Ln–O(21)	73.0(1)	73.6(2)
O(1)–Ln–O(31)	78.4(1)	78.0(2)	N(8)–Ln–O(31)	81.0(1)	81.3(2)
N(11)–Ln–O(31)	116.0(1)	116.1(2)	N(14)–Ln–O(31)	121.7(1)	121.8(2)
O(21)–Ln–O(31)	81.1(1)	80.4(2)	O(1)–Ln–O(32)	126.8(1)	126.9(2)
N(8)–Ln–O(32)	86.1(1)	87.4(3)	N(11)–Ln–O(32)	73.1(1)	73.2(2)
N(14)–Ln–O(32)	81.7(1)	81.3(2)	O(21)–Ln–O(32)	97.0(1)	96.4(2)
O(31)–Ln–O(32)	50.4(1)	50.7(2)	O(1)–Ln–O(1a)	71.3(1)	71.6(2)
N(8)–Ln–O(1a)	91.3(1)	90.8(2)	N(11)–Ln–O(1a)	86.7(1)	86.8(2)
N(14)–Ln–O(1a)	84.8(1)	84.8(2)	O(21)–Ln–O(1a)	94.5(1)	94.8(2)
O(31)–Ln–O(1a)	149.6(1)	149.4(2)	O(32)–Ln–O(1a)	158.9(1)	158.9(2)
Ln–O(1)–Ln(a)	108.7(1)	108.4(2)			

6° about the C(15)–C(16) bond. The loss of conjugation due to the rotation of the C(1)–C(6) aryl ring out of the plane of its adjacent C=N bond together with the different nucleating role of O(1) compared to O(21) results in significant differences in the associated C(aryl)–O bond distances, 1.348(4) Å to O(1) compared to 1.311(6) Å to O(21). There are no inter- or intramolecular ligand–ligand or aryl–aryl interactions or hydrogen bonds.

The ability to satisfy the co-ordination requirements of the Gd^{3+} centres with only eight co-ordinating atoms and without resort to additionally bound solvent molecules, especially water or alcohol, is an important consideration in the design of Ln^{3+} photonic devices since frequently such co-ordinated solvent molecules are efficient quenchers of Ln^{3+} luminescence.[17]

An investigation of the spatial distribution of the Gd^{3+} cations throughout the crystal shows the oxygen-bridged Gd^{3+} pairs to be well separated from their symmetry and lattice translated neighbours. The closest interdimer Gd···Gd distances are 7.94 and 8.14 Å. The (Gd^{3+}···Gd^{3+}) cation pairs being arrayed in parallel sheets (Fig. 3) separated by approximately 10.9 Å. The Ln^{3+}···Ln^{3+} cation pair in $[\{LnL^7(NO_3)_2\}_2]$ molecules is therefore suitable for investigation of Ln^{3+}···Ln^{3+} electronic interactions. An understanding of these interactions is essential for the design of tuning mechanisms for potential Ln^{3+} photonic devices and magnetic resonance imaging (MRI) contrast enhancement agents.[1]

Efficient photosensitization of Ln^{3+}

Upon excitation at 390 nm, the chelate L^7 exhibits a broad emission band in the region 450–600 nm (peaking at 520 nm) on to which sharp, weak Tb^{3+} ($^5D_4 \longrightarrow {}^7F_J$) peaks are superimposed (Fig. 4). The emission spectrum of the $[\{LuL^7(NO_3)\}_2]$·MeOH complex is dominated by Tb^{3+} ($^5D_4 \longrightarrow {}^7F_J$) emission peaks at 490 ($J = 6$), 545 ($J = 5$) and 585 nm ($J = 4$) and Eu^{3+} ($^5D_0 \longrightarrow {}^7F_J$) 585 ($J = 1$) and 610 nm ($J = 2$) (Fig. 4). The Tb^{3+} and Eu^{3+} species are present in the $[\{LnL^7(NO_3)\}_2]$ complexes (Ln = Lu or Gd) as trace impurities;[2] for example ICP analyses show $[\{LuL^7(NO_3)\}_2]$·MeOH to contain (ppm) Eu = 532; Tb < 100; Nd < 20; Yb < 20 while Lu = 31.7%. Ligand L^7 is therefore a good sensitizer for Ln^{3+} emission, particularly that of Tb^{3+} ($^5D_4$) which is very weak when Tb^{3+} ($^5D_4$) is directly excited at 488 nm. This conclusion is supported by the excitation spectra of Tb^{3+} ($^5D_4$) (λ_{em} = 544 nm), Eu^{3+} ($^5D_0$) (λ_{em} = 610 nm) and the chelate (λ_{em} = 563 nm) which generally show similar broad ligand absorptions in the region 270–430 nm (Figs. 4 and 5). The absorption spectra of $[\{LnL^7(NO_3)\}_2]$·*n*MeOH features broad peaks, typical of imino–phenolate chromophores at 34 200, 27 900, 26 500 cm^{-1} and a broad shoulder extending to lower energy (Fig. 6). Agreement between the ligand absorption frequencies in the excitation spectra of Tb^{3+} ($^5D_4$) and Eu^{3+} ($^5D_0$) emission (Figs. 4 and 5) and the absorption spectrum (Fig. 6) is good. We thus conclude that Tb^{3+} ($^5D_4$) emission, as in other systems studied previously,[1,2,5,6] is most efficiently sensitized by the singlet state[18] while Eu^{3+} ($^5D_0$) emission is sensitized by both the triplet (or n $\longrightarrow \pi^*$)[19] and the singlet states. In addition to ligand states f–f transitions are prominent in the Eu^{3+} sample while only a weak $^7F_6 \longrightarrow {}^5D_4$ absorption is found in Tb^{3+} (Fig. 5).

Further evidence for the sensitization of Tb^{3+} ($^5D_4$) and Eu^{3+} ($^5D_0$) emission by the ligand states is provided by the excitation build-up of *ca.* 30 μs seen on the Tb^{3+} ($^5D_4$) and Eu^{3+} ($^5D_0$) emission decay curves following ligand excitation in the UV but not when the metal states are excited directly at 488 and 575 nm respectively. The excitation build-up is followed by exponential decay behaviour; with Tb^{3+} and Eu^{3+} diluted in $[\{LuL^7(NO_3)\}_2]$·MeOH, the decay rates are 8.3×10^2 and 2.4×10^3 s^{-1} respectively. These parameters are reasonable since the N–H functionality, which is proximate to the Ln^{3+} (Fig. 1), is a good quencher for Tb^{3+} and Eu^{3+} emission.[20] When the quenching behaviour of N–H is considered[17,20] the decay rates of Eu^{3+} ($^5D_0$) emission, 2.4×10^3 s^{-1} in complexes of L^7 (which have one N–H per Ln^{3+}) and 3.3×10^3 s^{-1} in compounds of L^2 (ref. 21) (which have two N–H per Ln^{3+} ion), are found to be consistent. The chelate luminescence decay curves of $[\{GdL^7(NO_3)\}_2]$ (λ_{exc} = 337 nm, λ_{em} = 563 nm) at 77 K reveal an initial excitation build-up for about 25–30 μs, which is not found in the Lu^{3+} complex, followed by non-exponential decay. However, the tails are exponential after about 100 μs, with decay rates of $\approx 4.2 \times 10^3$ and 77 s^{-1} for Ln = Gd (paramagnetic) and Lu (diamagnetic), respectively. Due to complications expected from the significant dissimilarity of the imino–phenolate chromophores (see above and Fig. 1), further detailed interpretation of the luminescence spectra and decay kinetics of L^7 was not attempted.

Energy transfer among Ln^{3+} ions

Strong and moderately intense emissions are observed at 77 K from Tb^{3+} ($^5D_4$) and Eu^{3+} ($^5D_0$) respectively in dilute $[(Ln'_{1-x}Ln_x)L^7(NO_3)]_2$·*n*MeOH (Ln = Tb or Eu; Ln' = Gd or Lu; dilute $x < 0.01$, concentrated $x \approx 1$) and in concentrated $[\{LnL^7(NO_3)\}_2]$ complexes. The corresponding emission spectra (Fig. 5) are typical[4–6,10] for Tb^{3+} and Eu^{3+} ions in co-ordination environments of low symmetry[22] such as the C_{2v} LnO_3N_3 polyhedron found in $[\{LnL^7(NO_3)\}_2]$ (Fig. 2). Emission from Sm^{3+} and Dy^{3+} was sought but not found at 77 K.

Direct excitation of Tb^{3+} ($^5D_4$) (λ_{exc} 488 nm) and Eu^{3+} ($^5D_0$) (λ_{exc} 575 nm) at 77 K yields essentially exponential decay curves. The decay rates of both Eu^{3+} and Tb^{3+} emission are

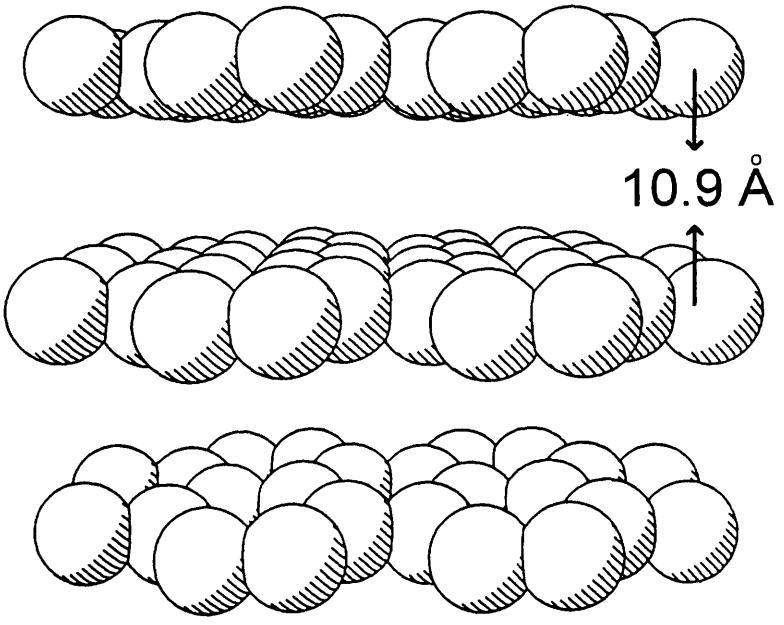

Fig. 3 The extended array of Ln · · · Ln pairs into parallel sheets

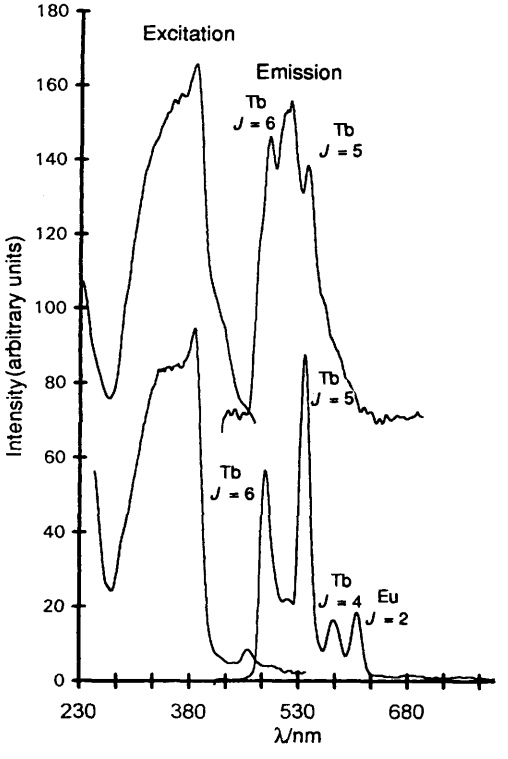

Fig. 4 The 77 K emission (λ_{ex} = 390 nm) and excitation (λ_{em} = 563 nm) spectra for Gd (top set) and Lu (bottom set) complexes of L^7 showing the intense ligand absorption leading to Tb^{3+} and Eu^{3+} impurity emission

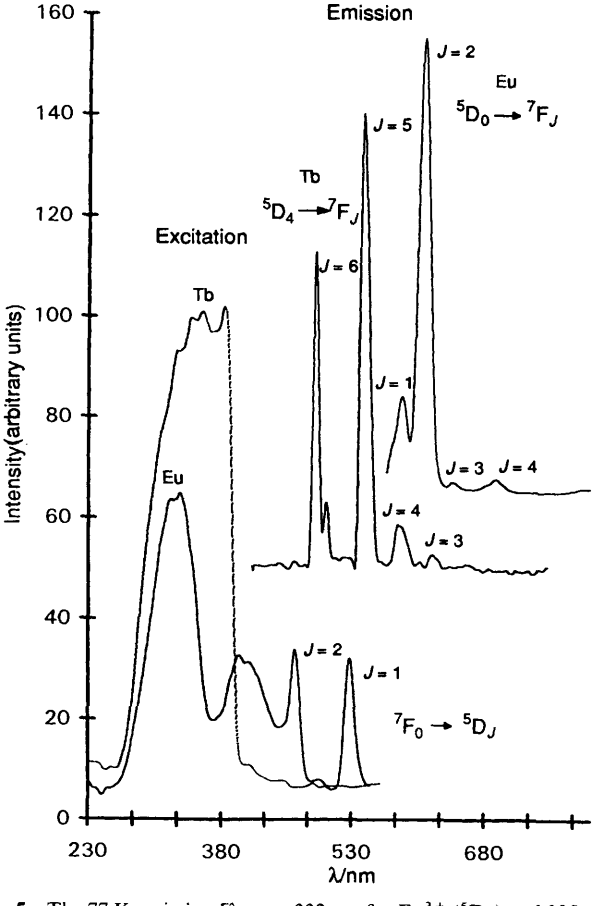

Fig. 5 The 77 K emission [λ_{exc} = 332 nm for Eu^{3+} ($^5D_0$) and 385 nm for Tb^{3+} ($^5D_4$)] and excitation [λ_{em} = 544 nm (Tb^{3+}) and 610 nm (Eu^{3+})]

slightly slower in the dilute samples, $[(Ln'_{1-x}Ln_x)L^7(NO_3)]\cdot n$MeOH (Ln' = Gd or Lu; Ln = Eu or Tb) compared to the concentrated ones, $[\{LnL^7(NO_3)\}_2]\cdot n$MeOH (Ln = Eu or Tb). For $[\{(Ln'_{1-x}Eu_x)L^7(NO_3)\}_2]\cdot n$MeOH the decay rates of Eu^{3+} ($^5D_0$) emission are 2.4×10^3 s^{-1} (Ln = Gd) and 2.3×10^3 s^{-1} (Ln = Lu) compared to 2.6×10^3 s^{-1} for $[\{EuL^7(NO_3)\}_2]$. With $[\{(Ln'_{1-x}Tb_x)L^7(NO_3)\}_2]\cdot$MeOH the decay rate is 8.1×10^2 for Ln = Lu compared to 1.0×10^3 s^{-1} for $[\{TbL^7(NO_3)\}_2]$. These small concentration quenching effects are indicative of weak $Eu^{3+} \longrightarrow Eu^{3+}$ and $Tb^{3+} \longrightarrow Tb^{3+}$ electronic coupling, and since the decay curves are almost exponential, both inter- and intra-molecular couplings are possible. For example, the decay curves of Eu^{3+} ($^5D_0$) emissions from a series of $[\{(Eu_{1-x}Dy_x)L^7(NO_3)\}_2]$ complexes exhibit marginal deviations from exponential behaviour (Fig. 7) while the quenched emission decay rates increase from 2.4×10^3 s^{-1} for $x = 0$, to 4.7×10^3 s^{-1} for $x = 0.85$. For the mixed europium–samarium complexes the decay rate of Eu^{3+}

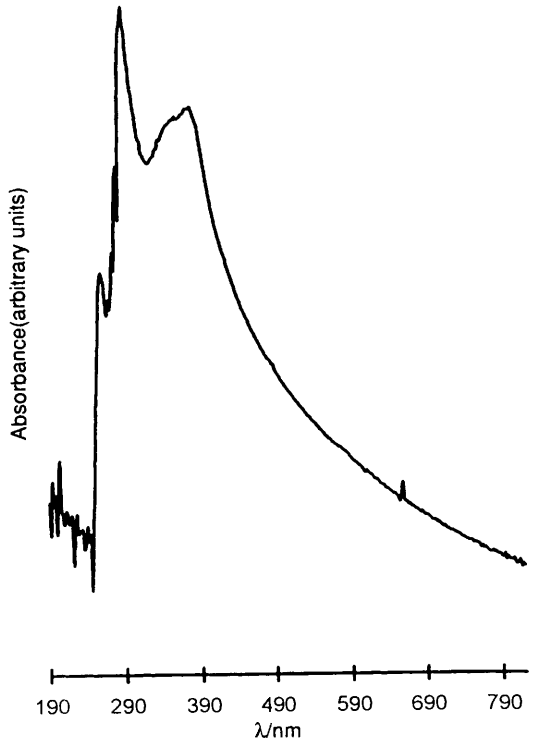

Fig. 6 Representative 298 K absorption spectrum for crystalline $[\{LnL^7(NO_3)\}_2]$ compounds in Nujol mull (spectrum for Ln = Dy is shown)

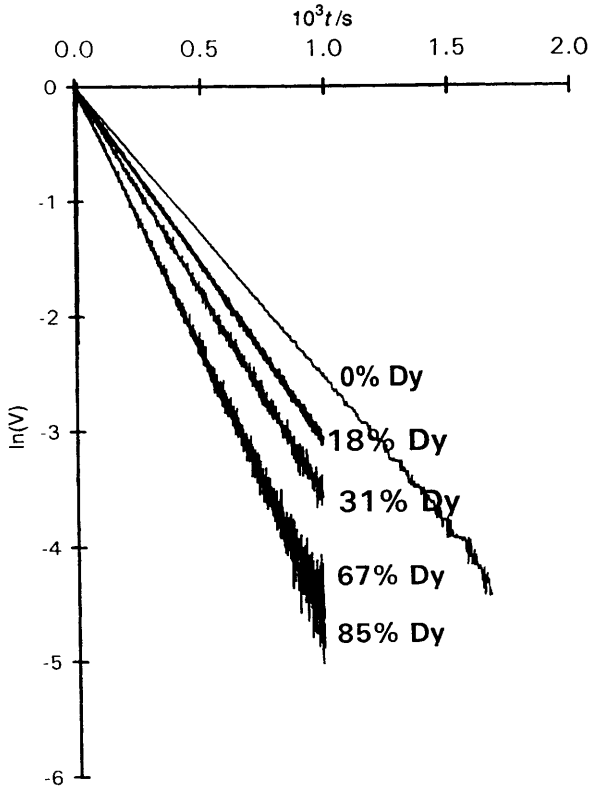

Fig. 7 The dependence of the decay curves of Eu^{3+} ($^5D_0$) emission on the concentration of Dy^{3+} in $[\{Eu_{1-x}Dy_x)L^7(NO_3)\}_2]$ at 77 K, λ_{exc} = 575 nm

($^5D_0$) emission increases to 5.8×10^3 s^{-1} for $x = 0.69$. The energy transport behaviour of the Eu^{3+} samples (Ln = Sm or Dy) is thus close to the dynamic regime described by Huber.[23] However, with more efficient traps like Nd^{3+}, fast $Eu^{3+} \longrightarrow Nd^{3+}$ energy transfer dominates and non-exponential behaviour prevails. Intramolecular Eu^{3+}–Ln^{3+} (Ln = Sm, Dy

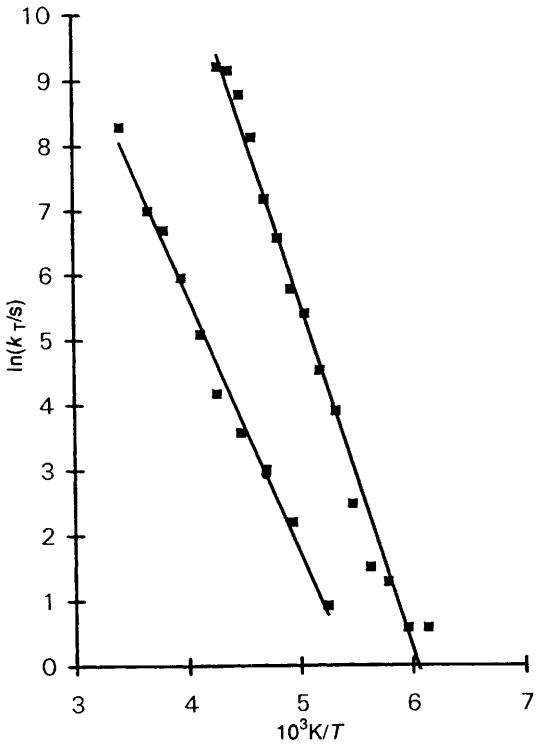

Fig. 8 The temperature evolution of the trapping rates of Eu^{3+} ($^5D_0$) (λ_{exc} = 575 nm) and Tb^{3+} ($^5D_4$) (λ_{exc} = 488 nm) excitation in crystalline $[\{LnL^7(NO_3)\}_2]$ (Ln = Tb or Eu)

or Nd) energy transfer rates are expected to be much higher than those found above (Fig. 7). Thus the observed asymptotically limiting decay rate ($k_o = 4.7 \times 10^3$ s^{-1}) for $[\{(Eu_{1-x}Dy_x)L^7(NO_3)\}_2]$ ($x = 0.85$) is due to intermolecular coupling involving Eu^{3+}–Eu^{3+} homopairs and nearest Dy^{3+}–Eu^{3+} and Dy^{3+}–Dy^{3+} neighbours. Assuming that the intermolecular coupling mechanism is predominantly dipolar ($k_T = \alpha/r^6$) the dipole–dipole Eu^{3+}–Dy^{3+} coupling constant[24] is estimated at $\alpha \approx 7 \times 10^{-52}$ m^6 s^{-1} which is in good agreement with the value of 6.8×10^{-52} m^6 s^{-1} derived from the Eu^{3+}–Dy^{3+} heteropair decay kinetics for complexes of L^1 (ref. 25) [$k_T = k_o - k_c$; k_T = Eu^{3+}–Dy^{3+} trapping rate; k_c = 2.6×10^3 s^{-1} = cumulative temperature independent decay rate (see below)]. Most probably resonant energy transfer (Fig. 9) is dominant and occurs *via* equations (3) and/or (4).

$$Eu^{3+}(^5D_0) + Dy^{3+}(^6H_{15/2}) \longrightarrow Eu^{3+}(^7F_6) + Dy^{3+}(^6F_{5/2}) \quad (3)$$

$$Eu^{3+}(^5D_0) + Dy^{3+}(^6H_{15/2}) \longrightarrow Eu^{3+}(^7F_5) + Dy^{3+}(^6F_{3/2}) \quad (4)$$

For $[(Eu_{1-x}Ln_x)_2 L^1(NO_3)_4]\cdot H_2O$ a static regime dominates and the non-exponential decay curves of Eu^{3+} ($^5D_0$) emission show distinctly the contributions of both intramolecular Eu^{3+}–Ln^{3+} heteropair and intermolecular (Eu^{3+}–Eu^{3+})•••(Eu^{3+}–Ln^{3+}) and (Eu^{3+}–Eu^{3+})•••(Ln^{3+}–Ln^{3+}) interactions.[7]

The emission decay rates of Tb^{3+} ($^5D_4$) ($T > 190$ K) and Eu^{3+} ($^5D_0$) ($T > 170$ K) are temperature dependent (Fig. 8) with thermal barriers of 2500 and 3600 cm^{-1} respectively. Whereas knowledge of these thermal characteristics is essential when considering potential applications in photonic devices, a satisfactory explanation is still lacking.[1,6] On the basis of previous observations on imino–phenolate chromophores[1,4–6] and Fig. 5 it is likely that thermalized quenching of both Eu^{3+} ($^5D_0$) and Tb^{3+} ($^5D_4$) emission is effected largely by ligand chromophore states [singlet for Tb^{3+} (origin ≈23 000 cm^{-1}) and triplet for Eu^{3+} (origin ≈21 000 cm^{-1})]. Thus, the thermal barriers correspond to the energy needed to bridge the Eu^{3+}

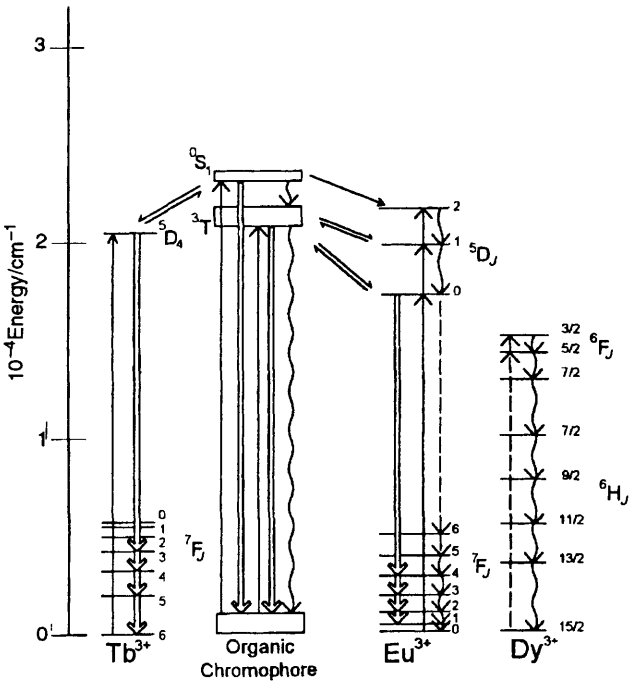

Fig. 9 A summary of possible energy transport processes for $[\{LnL^7(NO_3)\}_2]$. Energy of Dy^{3+} states are estimated[26] while the others are largely derived from spectral data (Fig. 5)

($^5D_0$) or Tb^{3+} ($^5D_4$) emitting states with the upper quenching ligand states as shown in Fig. 9. This conclusion is consistent with differences found in the mechanisms by which Tb^{3+} and Eu^{3+} couple to the ligand states (see above).

Conclusion

These studies have shown that greater dinuclear complex stability and enhanced interlanthanide cation electronic interactions, especially among similar Ln^{3+} cations, can be achieved by increasing the chelate negative charge to lanthanide cation ratio. High negatively charged anionic polynucleating chelates favour short $Ln^{3+} \cdots Ln^{3+}$ contacts and are therefore of great interest when complexes with strong Ln^{3+}–Ln^{3+} electronic interactions are desired.[1,7] Further, increasing the number of aromatic light gathering ('antenna') species leads to more efficient sensitization of Ln^{3+} emission.[27] These revelations should be helpful[28,29] in the design and preparation of complexes with potential applications as tunable Ln–Ln luminescent and diagnostic MRI contrast media and novel diagnostic/therapeutic agents employing two techniques simultaneously (*e.g.* radiology and fluorescence).

Acknowledgements

We thank the Leverhulme Trust for supporting the work at University of the West Indies (UWI). The British Council/UWI CICHE programme for supporting the UWI/Imperial College Collaboration and the Department of Chemistry for a Departmental award to R. C. H. We thank Charles Grant and Professor G. Lalor of the Centre for Nuclear Sciences (UWI) for help with NAA and the Forensic Laboratory (Jamaica) for the loan of the LS5 spectrometer.

References

1 K. D. Matthews, I. A. Kahwa and D. J. Williams, *Inorg. Chem.*, 1994, **33**, 1382.
2 I. A. Kahwa, S. Folkes, D. J. Williams, S. V. Ley, C. A. O'Mahoney and G. L. McPherson, *J. Chem. Soc., Chem. Commun.*, 1989, 1531.
3 J. M. Harrowfield, M. I. Ogden, A. H. White and F. R. Wilner, *Aust. J. Chem.*, 1989, **42**, 949; J. M. Harrowfield, M. I. Ogden and A. H. White, *Aust. J. Chem.*, 1991, **44**, 1237, 1249; B. M. Furphy, J. M. Harrowfield, D. L. Kepert, B. W. Skelton, A. H. White and F. R. Wilner, *Inorg. Chem.*, 1987, **26**, 4231.
4 I. A. Kahwa, J. Selbin, T. C.-Y. Hsieh and R. A. Laine, *Inorg. Chim. Acta*, 1986, **118**, 179.
5 P. Guerriero, P. A. Vigato, J.-C. G. Bünzli and E. Moret, *J. Chem. Soc., Dalton Trans.*, 1990, 647.
6 K. D. Matthews, S. A. Bailey-Folkes, I. A. Kahwa, C. A. O'Mahoney, S. V. Ley, D. J. Williams, C. J. Groombridge and C. J. O'Connor, *J. Phys. Chem.*, 1992, **96**, 7021.
7 K. D. Matthews, R. A. Fairman, A. Johnson, K. V. N. Spence, I. A. Kahwa, G. L. McPherson and H. Robotham, *J. Chem. Soc., Dalton Trans.*, 1993, 1719.
8 P. Guerriero, U. Casellato, S. Tamburini, P. A. Vigato and R. Graziani, *Inorg. Chim. Acta*, 1987, **129**, 127.
9 J.-C. G. Bünzli, E. Moret, U. Casellato, P. Guerriero and P. A. Vigato, *Inorg. Chim. Acta*, 1988, **150**, 133.
10 P. Guerriero, P. A. Vigato, D. E. Fenton and P. C. Hellier, *Acta Chem. Scand.*, 1992, **46**, 1025.
11 H.-J. Schneider, *Angew. Chem., Int. Ed. Engl.*, 1991, **30**, 1417.
12 R. F. Lauffer, *Chem. Rev.*, 1987, **87**, 901; W. P. Cacheris, S. C. Quaysand and J. M. Rocklage, *Magn. Reson. Imaging*, 1990, **8**, 467.
13 C. F. Meares and T. G. Wensel, *Acc. Chem. Res.*, 1984, **17**, 202.
14 R. D. Hancock, I. Cukrowski, E. Cukrowska, G. D. Hosken, V. Iccharam, M. W. Brechbiel and O. A. Gansow, *J. Chem. Soc., Dalton Trans.*, 1994, 2679.
15 G. M. Sheldrick, SHELTXL PC version 4.2, Siemens Analytical X-Ray Instruments Inc., Madison, WI, 1990.
16 H. C. Aspinall, J. Black, I. Dodd, M. M. Harding and S. J. Winkley, *J. Chem. Soc., Dalton Trans.*, 1993, 709.
17 W. DeW. Horrocks, jun. and D. R. Sudnick, *Acc. Chem. Res.*, 1981, **14**, 384.
18 M. Klinerman, *J. Chem. Phys.*, 1969, **51**, 2370.
19 H. Durr and B. Ruge, *Top. Curr. Chem.*, 1976, **66**, 53; S. K. Mandal and K. J. Nag, *J. Chem. Soc., Dalton Trans.*, 1984, 2141.
20 Z. Wang, G. R. Choppin, P. D. Bernardo, P.-L. Zanonato, R. Portanova and M. Tolazzi, *J. Chem. Soc., Dalton Trans.*, 1993, 2791.
21 I. A. Kahwa, J. Selbin, C. J. O'Connor, J. W. Foise and G. L. McPherson, *Inorg. Chim. Acta*, 1988, **148**, 265.
22 G. Blasse, *Recl. Trav. Chim. Pays-Bas*, 1986, **105**, 143; J. H. Forsberg, *Coord. Chem. Rev.*, 1973, **10**, 195; S. P. Sinha and E. Butter, *Mol. Phys.*, 1969, **16**, 285.
23 D. L. Huber, *Phys. Rev. B*, 1979, **20**, 2307, 5333.
24 T. Föster, *Z. Naturforsch.*, 1949, **49**, 321; L. Dexter, *J. Chem. Phys.*, 1953, **21**, 836.
25 K. D. Matthews, Ph.D. Thesis, University of the West Indies, Mona, Kingston, 1994.
26 G. H. Dieke, *Spectra and Energy Levels of Rare Earth Ions in Crystals*, ed. H. M. Crosswhite and H. Crosswhite, Interscience, 1968, p. 142.
27 B. Alpha, R. Ballardini, V. Balzani, J.-M. Lehn, S. Perathoner and N. Sabatini, *Photochem. Photobiol.*, 1990, **52**, 299.
28 P. Guerriero, S. Tamburini and P. A. Vigato, *Coord. Chem. Rev.*, 1995, **139**, 17.
29 V. Alexander, *Chem. Rev.*, 1995, **95**, 273.

Received 5th July 1995; *Paper* 5/04350F